Electro-optical tunable time delay and advance in a silicon feedback-microring resonator

Shaoqi Feng,[1] Xianshu Luo,[1,3] Shengwang Du,[2] and Andrew W. Poon[1,*]

[1]*Photonic Device Laboratory, Department of Electronic and Computer Engineering, The Hong Kong University of Science and Technology, Clear Water Bay, Hong Kong SAR, China*

[2]*Department of Physics, The Hong Kong University of Science and Technology, Clear Water Bay, Hong Kong SAR, China*

[3]*Current address: Institute of Microelectronics, A*STAR (Agency of Science, Technology and Research), 11 Science Park Road, Singapore Science Park II, Singapore 117685*

**Corresponding author: eeawpoon@ust.hk*

Received January 4, 2011; revised March 1, 2011; accepted March 4, 2011; posted March 7, 2011 (Doc. ID 140433); published March 31, 2011

We report the demonstration of electro-optical tunable time delay and advance using a silicon feedback-microring resonator integrated with p-i-n diodes. By controlling the feedback and round-trip phase shifts through the carrier-injection-based free-carrier dispersion effect, we obtain a large dynamic time tuning range (–88 ps to 110 ps) upon dc bias voltage change in the range of few tens of millivolts at a given resonance wavelength. We also demonstrate tunable time delay and advance at different resonance wavelengths within 0.76 nm wavelength range. © 2011 Optical Society of America

OCIS codes: 230.5750, 130.3120, 230.3990.

Controllable optical time delay has attracted much research interest during the past decade because of its key role in realizing all-optical networks and high-speed optical information processing [1,2]. Slow- and fast-light techniques can also be applied to true time-delay phased antenna arrays for beam steering and shaping [2], as well as to improving the spectral sensitivity of interferometers [3]. Recently, silicon-microresonator-based slow- and fast-light devices have been of particular interest due to their compatibility for on-chip optical integration [4–9]. The tunability of these silicon-based devices is realized via either thermo-optical [4–8] or electro-optical [9] effect. However, in previous demonstrations, separate tuning of time delay and resonance wavelength has not been realized.

In this Letter, we demonstrate that time delay and resonance wavelength can be controlled separately in a silicon feedback-microring resonator. Figure 1(a) shows the schematic of a p-i-n diode-integrated feedback-microring resonator [10,11]. The device comprises a single microring resonator laterally coupled to a feedback waveguide with two waveguide directional couplers. Light is launched from the input waveguide, partially coupled into the microring resonator and partially transmitted to the feedback waveguide. The light fields transmitted from the microring resonator and the feedback waveguide interfere with each other at the output waveguide. Under the microring resonator approximation (the feedback waveguide is weakly coupled to the microring) [11], the resonances are determined by the microring resonator, while the output intensity and the phase response can be tuned by changing the phase shift through the feedback waveguide. In order to attain electrically reconfigurable intensity and phase response, both the microring resonator and part of the feedback waveguide are laterally integrated with p-i-n diodes, which are denoted as diodes R and U. By forward-biasing the diodes, we obtain refractive index change in the intrinsic waveguide region due to the free-carrier dispersion (FCD) effect [12]. Forward-biasing the diode U with voltage V_U, we change the phase shift through the feedback waveguide, and thus control the intensity and phase responses. Forward-biasing the diode R with voltage V_R, we change the round-trip phase shift within the microring resonator, and thus blueshift the resonance wavelength. Therefore, we tune the time delay and the resonance

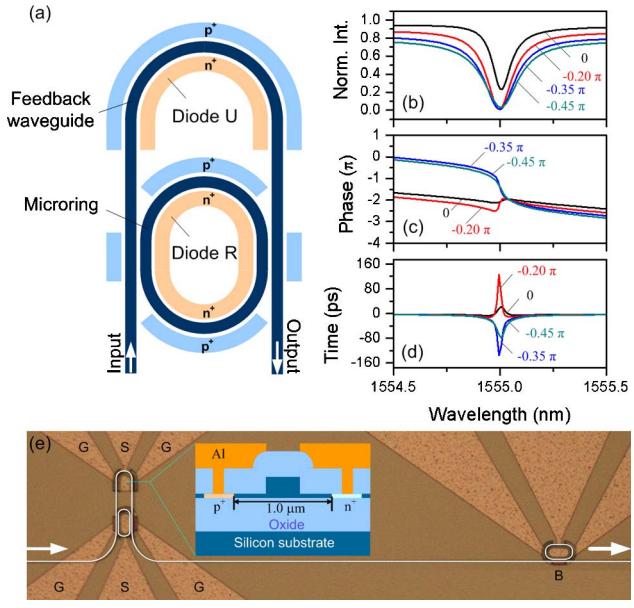

Fig. 1. (Color online) (a) Schematic of a silicon feedback-microring resonator with laterally integrated p-i-n diodes in a SOI substrate. (b)–(d) Modeled normalized intensity (b), phase response (c), and time delay (d) upon various feedback-phase shift $\delta\psi$ of 0 (black), -0.20π (red), -0.35π (blue), and -0.45π (green). (e) Optical micrograph of the fabricated device comprising the feedback-microring resonator connected to a microring-resonator-based notch filter without the feedback waveguide. G, ground; S, signal. Inset: schematic cross section of the diode-integrated waveguide. Al, aluminum.

wavelength separately by such structure, whereas in the conventional structure of a single waveguide-coupled ring resonator, the typical method of tuning the time delay via phase shifting the ring resonator (as in [9]) necessarily shifts the resonance wavelength.

We model our p-i-n diode-integrated feedback-microring resonator using a transfer-matrix method [11]. The input-normalized electric field transmission is expressed as

$$\frac{E_{\text{out}}}{E_{\text{in}}} = \frac{\tau^2 b\gamma e^{-i(\psi+2\varphi)} - \kappa^2 a\eta e^{-i(\theta+2\varphi)} - a^2\eta^2 b\gamma e^{-i(2\theta+\psi+4\varphi)}}{1 + \kappa^2 a\eta b\gamma e^{-i(\theta+\psi+2\varphi)} - \tau^2 a^2\eta^2 e^{-i(2\theta+2\varphi)}}, \tag{1}$$

where κ and τ are the coupling and transmission coefficients of the waveguide directional couplers, φ is the transmission phase change of the couplers, a is the field transmission factor for the 180° arc of the racetrack ring, η is the field transmission factor for the 180° arc under free-carrier absorption, $\theta = \theta_0 + \delta\theta$ is the 180° arc phase change comprising an initial phase change θ_0 and a free-carrier-induced phase shift $\delta\theta$, b is the feedback-waveguide field transmission factor, γ is the feedback-waveguide field transmission factor under free-carrier absorption, and $\psi = \psi_0 + \delta\psi$ is the feedback-waveguide phase change comprising an initial phase change ψ_0 and a free-carrier-induced phase shift $\delta\psi$. We note that θ_0, ψ_0, and φ are related with the 180° arc length L_a, the feedback-waveguide length L_b and the waveguide directional coupling length L_c as $\theta_0 = n_{\text{eff}} L_a(2\pi/\lambda)$, $\psi_0 = n_{\text{eff}} L_b(2\pi/\lambda)$, and $\varphi = n_{\text{eff}} L_c(2\pi/\lambda)$, where n_{eff} is the waveguide effective refractive index and λ is the free-space wavelength. We calculate the time delay by $\Delta t = -d\Phi/d\omega = (\lambda^2/2\pi c)d\Phi/d\lambda$, where Φ is the relative optical phase of the device transmission, given as $\Phi = \arg(E_{\text{out}}/E_{\text{in}})$, and c is the speed of light in free space.

Figures 1(b)–1(d) show the modeled normalized intensity, phase response, and time delay upon various free-carrier-induced feedback-waveguide phase shift $\delta\psi = 0$, -0.20π, -0.35π, and -0.45π (the negative phase shift is due to reduction of the refractive index by the FCD effect). Here we choose the following modeling parameters according to the device design parameters (satisfying the phase-matched feedback condition [11]): $L_a = 47\,\mu$m, $L_b = 183\,\mu$m, and $L_c = 20\,\mu$m; and based on fitting the measured spectra: $n_{\text{eff}} = 2.65$, $\kappa = 0.25$, $a = 0.97$, and $b = 0.97$. The modeling reveals that the resonance wavelengths are nearly fixed upon different $\delta\psi$. The resonance wavelengths are determined by the round-trip phase shift within the microring resonator yet not affected by the feedback-waveguide phase shift under the microring resonator approximation [11]. At $\delta\psi = 0$, the resonance displays an anomalous phase response and time advance, suggesting that the resonator operates in the undercoupling regime [9,13]. With increased $\delta\psi = -0.20\pi$, the resonances exhibit larger extinction ratio and time advance. At $\delta\psi = -0.35\pi$, the resonance shows a normal phase response and time delay, indicating that the resonator operates in the overcoupling regime. With further increased $\delta\psi = -0.45\pi$, the resonance lineshape is broadened and the time delay is compromised. Thus, by tuning $\delta\psi$, we control the coupling regime in the resonator, and thus obtain tunable intensity and phase responses and thereby, the time delay.

We fabricate the device on a silicon-on-insulator (SOI) wafer with a 0.34-μm-thick silicon device layer on a 1-μm-thick buried-oxide layer. We pattern the device using i-line (365 nm) photolithography followed by CF_4-based plasma etching process. The rib waveguide and the microring have a designed waveguide width of 0.4 μm. The gap spacing between the waveguide and the microring is 0.35 μm. The racetrack microring is designed with arc radius of 15 μm and interaction lengths of 20 μm. The intrinsic region width of the integrated lateral p-i-n diode across the microring and the feedback waveguide is 1 μm [Fig. 1(e), inset]. The length of the feedback waveguide L_b is 183 μm with 87 μm of the waveguide surrounded by the lateral p-i-n diode. Figure 1(e) shows the optical micrograph of the fabricated device comprising the feedback-microring resonator connected to a microring-resonator-based notch filter without the feedback waveguide (denoted as B). All the optical transmission spectra are measured after device B.

We measure the intensity and the time delay with the phase-shift technique [9]. We adopt 1 GHz modulation frequency, which gives rise to a maximum measurable delay of $\pm$500 ps and time resolution of ~10 ps. Figures 2(a)–2(c) show the measured TE-polarized (electric field parallel to the chip) transmission spectra and Figs. 2(d)–2(f) show the corresponding time delay upon $V_U = 0.00$ V, 1.00 V, and 1.01 V (with a wavelength resolution of 20 pm). We observe two sets of resonances in the transmission spectra, namely set A ($Q \sim 5000$) from the feedback-microring and set B from the single microring (as a control). The measured transmission spectra are normalized to the intensity at an off-resonance wavelength. We note that in Fig. 2(c) we observe splitting at resonance A upon this particular feedback phase, which we attribute to possible scattering-induced coupling and which requires further investiga-

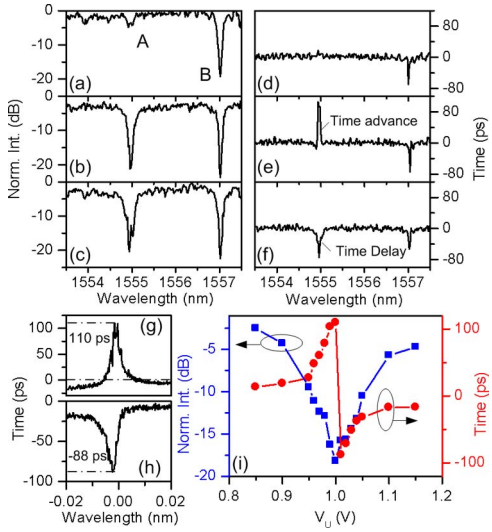

Fig. 2. (Color online) Measured (a)–(c) TE-polarized transmission spectra and (d)–(f) the corresponding time delay. (a), (d) $V_U = 0.00$ V; (b), (e) $V_U = 1.00$ V; (c), (f) $V_U = 1.01$ V. (g), (h) Zoom-in view of (e), (f) in the vicinity of resonance A. (i) Measured normalized intensity (blue squares) and time delay (red circles) of resonance A as a function of bias voltage V_U.

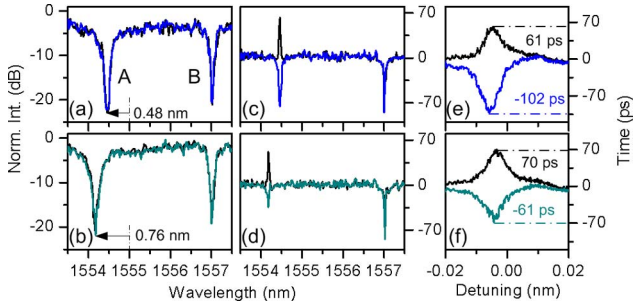

Fig. 3. (Color online) Measured (a)–(b) TE-polarized transmission spectra and (c)–(d) the corresponding time delay. (a), (c) $V_R = 0.95\,\mathrm{V}$, $V_U = 1.13\,\mathrm{V}$ (black), $V_U = 1.14\,\mathrm{V}$ (blue); (b), (d) $V_R = 1.00\,\mathrm{V}$, $V_U = 1.18\,\mathrm{V}$ (black), $V_U = 1.20\,\mathrm{V}$ (green). (e), (f) Zoom-in view of (c), (d) in the vicinity of resonance A.

tion. Figures 2(g) and 2(h) show the measured time delay and advance in the vicinity of resonance wavelength A with a wavelength resolution of 2 pm upon $V_U = 1.00\,\mathrm{V}$ and 1.01 V.

Figure 2(i) summarizes the measured intensity and time delay as a function of V_U at resonance wavelength of 1554.94 nm. Upon V_U from 0.85 V to 1.00 V, the intensity drops to a minimum of −18 dB while the time advance increases to 110 ps. Upon V_U from 1.00 V to 1.01 V, the intensity remains near the minimum while the observed maximum time advance transits to a maximum time delay of −88 ps. Upon V_U from 1.01 V to 1.15 V, the intensity rises to −5 dB while the time delay reduces to ∼10 ps.

The device shows a delay bandwidth (FWHM delay) of ∼1.5 GHz at the maximum delay, suggesting a delay-bandwidth product (DBP) of ∼0.132. In comparison, our previously demonstrated device of a single waveguide-coupled microring resonator [9] showed a delay bandwidth of ∼3.5 GHz with a maximum delay of −95 ps, which gave a DBP of ∼0.3. Other silicon single microring resonator-based devices have demonstrated a DBP of ∼0.5, albeit using transmission intensity bandwidth [4]. The narrowband characteristic of the above single ring devices, however, imposes a significant limitation that compromises their actual use for optical signal processing in high-speed networks. The large group-velocity dispersion within the bandwidth can cause a significant signal distortion. One of the possible mitigations is to cascade multiple feedback-microring resonators in order to broaden the bandwidth [7,8].

We emphasize that the key benefit of such feedback-microring resonators is that one can separate tuning of the microring resonance wavelength from tuning of the transmission intensity and the time delay. Figure 3 shows the measured feedback-controlled resonance transmission [Figs. 3(a) and 3(b)] and the corresponding time delay [Figs. 3(c) and 3(d)] at blueshifted resonance wavelengths upon various bias voltages. Upon $V_R =$ 0.95 V, the resonance wavelength blueshifts by ∼0.48 nm with respect to the 1554.94 nm resonance wavelength. We observe 61 ps advance and −102 ps delay with $V_U = 1.13\,\mathrm{V}$ and 1.14 V. Upon $V_R = 1.00\,\mathrm{V}$, the resonance wavelength blueshifts by ∼0.76 nm with respect to the 1554.94 nm resonance wavelength. We measure 70 ps advance and −61 ps delay with $V_U = 1.18\,\mathrm{V}$ and 1.20 V.

In summary, we demonstrated an electro-optical tunable time delay using a silicon feedback-microring resonator integrated with p-i-n diodes. We obtained a large dynamic time tuning range (−88 ps to 110 ps) upon dc biasing of the diode-integrated feedback waveguide in the range of few tens of millivolts at a given resonance wavelength. We also demonstrated a tunable time delay at blueshifted resonance wavelengths within the 0.76 nm range. Compared with previous demonstrations [4–9], we believe that the separate tuning of time delay and resonance wavelength offers additional flexibility for on-chip time-delay/advance applications, and the electro-optical tuning enables fast nanosecond-speed switching.

This study was substantially supported by a grant from the Research Grants Council of The Hong Kong Special Administrative Region, China, under project no. 618707. The authors gratefully acknowledge The Hong Kong University of Science and Technology (HKUST) Nanoelectronics Fabrication Facility for the silicon chip nanofabrication.

References

1. R. W. Boyd and D. J. Gauthier, Prog. Opt. **43**, 497 (2002).
2. E. Parra and J. R. Lowell, Opt. Photonics News **18**, 40 (2007).
3. Z. Shi, R. W. Boyd, R. M. Camacho, P. K. Vudyasetu, and J. C. Howell, Phys. Rev. Lett. **99**, 240801 (2007).
4. Q. Li, F. F. Liu, Z. Y. Zhang, M. Qiu, and Y. K. Su, J. Lightwave Technol. **26**, 3744 (2008).
5. S. Manipatruni, P. Dong, Q. Xu, and M. Lipson, Opt. Lett. **33**, 2928 (2008).
6. H. P. Uranus, L. Zhuang, C. G. H. Roeloffzen, and H. J. W. M. Hoekstra, Opt. Lett. **32**, 2620 (2007).
7. A. Melloni, A. Canciamilla, C. Ferrari, F. Morichetti, L. O'Faolain, T. F. Krauss, R. De La Rue, A. Samarelli, and M. Sorel, IEEE Photon. J. **2**, 181 (2010).
8. J. Cardenas, M. A. Foster, N. Sherwood-Droz, C. B. Poitras, H. L. R. Lira, B. Zhang, A. L. Gaeta, J. B. Khurgin, P. Morton, and M. Lipson, Opt. Express **18**, 26525 (2010).
9. X. Luo, H. Chen, and A. W. Poon, Opt. Lett. **35**, 2940 (2010).
10. M. S. Rasras, D. M. Gill, S. S. Patel, K. Y. Tu, Y. K. Chen, A. E. White, A. T. S. Pomerene, D. N. Carothers, M. J. Grove, D. K. Sparacin, J. Michel, M. A. Beals, and L. C. Kimerling, J. Lightwave Technol. **25**, 87 (2007).
11. L. Zhou and A. W. Poon, Opt. Express **15**, 9194 (2007).
12. R. Soref and B. Bennett, IEEE J. Quantum Electron. **23**, 123 (1987).
13. J. Heebner, V. Wong, A. Schweinsberg, R. Boyd, and D. Jackson, IEEE J. Quantum Electron. **40**, 726 (2004).